Physics of the Dark Universe 4 (2014) 6–9

Contents lists available at ScienceDirect

Physics of the Dark Universe

journal homepage: www.elsevier.com/locate/dark

Precision measurements of e^+ e^- in Cosmic Ray with the Alpha Magnetic Spectrometer on the ISS

Roberto Battiston *, on behalf of the AMS Collaboration [1]

Dipartimento di Fisica Università di Trento e INFN-TIFPA, Via Sommarive 14, 38123 Povo, Italy

ARTICLE INFO

Keywords:
Cosmic rays
Space research
Dark matter
Antimatter

ABSTRACT

One hundred years after their discovery by Victor Hess, Cosmic Rays are nowadays subject of intense research from space based detectors, able to perform for the first time high precision measurement of their composition and spectra as well as of isotropy and time variability. On May 2011, the Alpha Magnetic Spectrometer (AMS-02), has been installed on the International Space Station, to measure with high accuracy the Cosmic Rays properties searching for rare events which could be indication of the nature of Dark Matter or presence of nuclear Antimatter. AMS-02 is the result of nearly two decades of effort of an international collaboration, to design and build a state of the art detector capable to perform high precision Cosmic Rays measurement. In this paper I will briefly report on the first results of AMS-02 two years after the beginning of the operations in space.

1. The AMS-02 detector on the ISS

The Alpha Magnetic Spectrometer, AMS-02, is a general purpose high energy particle physics detector. It was installed on the International Space Station (ISS), on 19 May 2011 (Fig. 1) to conduct a unique long duration mission (~20 years) of fundamental physics research in space.

The layout of the AMS-02 detector is shown in Fig. 2 presenting the event display of a 369 GeV positron recorded by AMS. It consists of nine planes of precision Silicon Tracker, a Transition Radiation Detector (TRD), four planes of Time of Flight counters (ToF), a permanent magnet, an array of AntiCoincidence Counters (ACC) surrounding the inner tracker, a Ring imaging Cherenkov detector (RICH), and an Electromagnetic Calorimeter (ECAL).

The TRD is designed to use transition radiation to distinguish between electrons and protons, and dE/dx to independently identify nuclei. It consists of 5248 proportional tubes of 6 mm diameter with a maximum length of 2 m arranged side by side in 16-tube modules. The 328 modules are mounted in 20 layers. Each layer is interleaved with a 20 mm thick fiber fleece radiator (LRP375) with a density of 0.06 g/cm^3. There are 12 layers of proportional tubes along the y axis located in the middle of the TRD and, along the x axis, four layers located on top and four on the bottom. The tubes are filled with a 90:10 Xe:CO_2 mixture. In order to differentiate between electron and protons, signals from all the TRD layers are combined in a log-likelihood probability of the electron (TRD-LL$_e$) or proton (TRD-LL$_p$) hypothesis. The ratio of these probabilities has been used in the AMS-02 positron fraction as e/p discriminator.

The Silicon Tracker measures the particle rigidity ($R = p/Z$), its charge sign and evaluates the absolute charge magnitude (Z). Rigidity and sign are derived from the measurement of the curvature of the particle in the 1.4 kG AMS magnetic field. Particle trajectory is determined by the coordinate measurement along the 9 layers (L1, ..., L9) of 300 μm thick double-side micro-strip Silicon sensors. With a spatial resolution of about 7 μm ($2 < Z < 6$) and a maximum lever arm of about 3 m for $Z > 1$, the maximum detectable rigidity (MDR), i.e. R corresponding to $\Delta R/R = 100\%$, is estimated to be around 3 TV. Each Tracker layer delivers an estimation of the particle charge magnitude from the energy deposition measurement ($\propto Z^2$) in a wide charge range $1 < Z < 26$. The 7 independent measurement of charge in the Inner tracker (from L2 to L8) can be combined together achieving a charge resolution of 0.12 charge units (c.u.) for Carbon.

Two planes of TOF counters are located above and two planes below the magnet. Each plane contains eight or ten scintillating paddles. Each paddle is equipped with two or three photomultiplier tubes on each end for efficient detection of traversing particles. The average time resolution of each counter has been measured to be 160 ps, and the overall velocity ($\beta = v/c$) resolution of the system has been measured to be 4% for $\beta = 1$,

* Tel.: +39 0461 28 1590.
E-mail address: roberto.battiston@unitn.it.

[1] For the complete list of the AMS Collaboration see Ref. [1].

http://dx.doi.org/10.1016/j.dark.2014.05.002

Fig. 1. The Alpha Magnetic Spectrometer installed on the ISS.

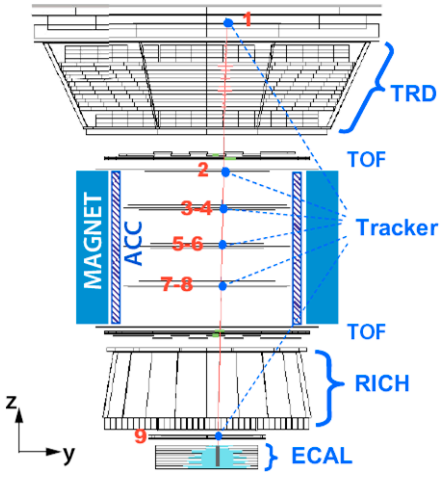

Fig. 2. A 369 GeV positron event as measured by the AMS detector on the ISS in the $(y–z)$ plane. Tracker planes 1–9 measure the particle charge $(+1)$ and momentum. The TRD identifies the particle as an electron/positron. The ToF measures the charge and ensures that the particle is downward-going. The RICH measures the charge and velocity. The ECAL independently identifies the particles an electron/positron and measures its energy.

$Z = 1$ particles. The ToF also discriminates between downward and upward-going particles. The coincidence of signals from all four ToF planes provides the charged particle trigger.

The ECAL consists of a multilayer sandwich of lead and scintillating fibers with an active area of 648 × 648 mm^2 and a thickness of 166.5 mm corresponding to 17 radiation lengths. The calorimeter is composed of nine superlayers, each 18.5 mm thick. In each superlayer, the fibers run in one direction only. The 3D imaging capability of the detector is obtained by stacking alternate superlayers with fibers parallel to the x and y axes (five and four superlayers, respectively). The fibers are read out on one end by 1296 photosensors with a linearity of 1/105 per sensor. Signals from three superlayers in y view (superlayers 2, 4, 6) and in x view (superlayers 1, 3, 5) are used in the trigger logic to select events with a shower in the calorimeter.

In the measurement of electrons and positron particles, the ToF detector is used to select $Z = 1$ relativistic particles traversing the AMS-02 in the downward direction with respect the AMS-02 reference system. The different characteristics of the signal released by protons, nuclei and electrons in the TRD and ECAL detectors are used to identify the electron component. A track reconstructed at least in the inner tracker (planes 2 to 8) and matching the TRD and ECAL signals is used to select clean $Z = 1$ events in the apparatus. Specific calibration procedures of all sub-detectors have been developed in order to guarantee the stability of the AMS-02 performances over time and no significant degradation of the apparatus has been observed during two years of operation in space.

2. Precision e^+ e^- physics with AMS

2.1. Positron to electron ratio

The AMS experiment collects about 1.5 billion Cosmic Ray during each month of operation. Results reported so far are based on the data collected during the initial 18 months of operations on the ISS, from 19 May 2011 to 10 December 2012. This constitutes 8% of the expected AMS data sample.

The first results published by the AMS Collaboration has been the precision measurement of the positron ratio from 0.5 to 350 GeV of energy [1]. The measured positron fraction is presented in Fig. 3 as a function of the reconstructed energy at the top of the AMS detector. As seen in the figure, below 10 GeV the positron fraction decreases with increasing energy as expected from the secondary production of cosmic rays by collision with the interstellar medium.

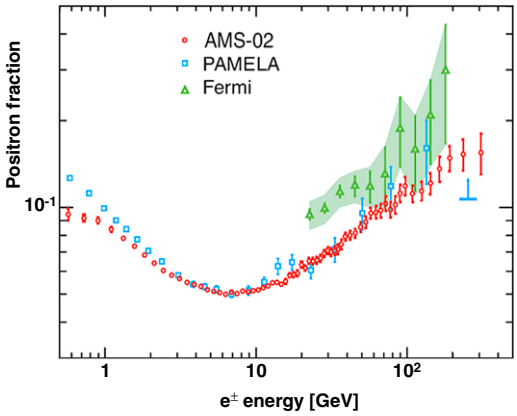

Fig. 3. The positron fraction compared with the most recent measurements from PAMELA [7] and Fermi-LAT [8]. The error bars for AMS are the quadratic sum of the statistical and systematic uncertainties and the horizontal positions are the centers of each bin.

The positron fraction is steadily increasing from 10 to ∼250 GeV. This is not consistent with only the secondary production of positrons [2]. The behavior above 250 GeV will become more transparent with more statistics which will also allow improved treatment of the systematic.

The observation of the positron fraction increase with energy has been reported by earlier experiments: TS93 [3], Wizard/CAPRICE [4], HEAT [5], AMS-01 [6], PAMELA [7] and Fermi-LAT [8]. The most recent results are presented in Fig. 3 for comparison. The accuracy of AMS-02 and high statistics available enable the reported AMS-02 positron fraction spectrum to be clearly distinct from earlier work (see Fig. 4). The AMS-02 positron ratio spectrum has the unique accuracy and energy range to provide accurate information on new phenomena.

The accuracy of the data enables us to investigate the properties of the positron fraction with different models. We did compare our data with a minimal model, as an example. In this model the e^+ and e^- fluxes, Φ_{e+} and Φ_{e-}, are parameterized as the sum of individual diffuse power law spectra and the contribution of a single common source of $e^{\pm}$

$$\Phi_{e+} = C_{e+}E^{-\gamma_{e+}} + C_s E^{-\gamma_s} e^{-E/Es}; \quad (1)$$

$$\Phi_{e-} = C_{e-}E^{-\gamma_{e-}} + C_s E^{-\gamma_s} e^{-E/Es}, \quad (2)$$

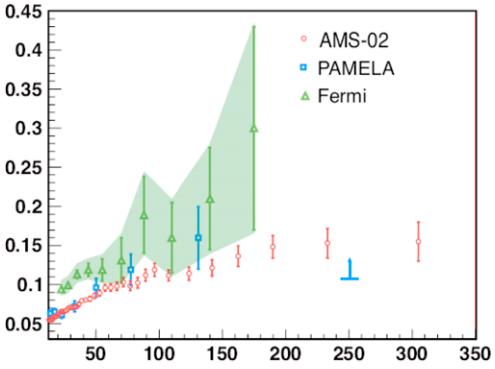

Fig. 4. The positron fraction at energies above 10 GeV compared with the most recent measurements from PAMELA [7] and Fermi-LAT [8]. AMS data clearly show the change in the behavior of the positron fraction in this energy range.

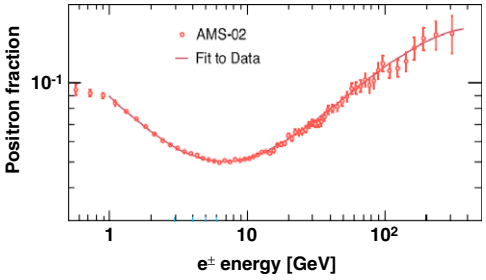

Fig. 5. The positron fraction measured by AMS fitted to the minimal model. For the fit, both the data and the model are integrated over the bin width. Even with the high statistics and high accuracy of AMS, the spectrum shows no fine structure.

(with E in GeV) where the coefficients C_{e+} and C_{e-} correspond to relative weights of diffuse spectra for positrons and electrons and C_s to the weight of the source spectrum; γ_{e+}, γ_{e-} and γ_s are the corresponding spectral indexes; Es is a characteristic cutoff energy for the source spectrum. With this parameterization the positron fraction depends on 5 parameters.

A fit to the data in the energy range 1 to 350 GeV based on the number of events in each bin yields a $\chi^2/df = 28.5/57$ and $\gamma_{e+} - \gamma_{e-} = -0.63 \pm 0.03$, i.e., the diffuse positron spectrum is softer, that is, less energetic with increasing energy, than the diffuse electron spectrum; $\gamma_{e-} - \gamma_s = 0.66 \pm 0.05$, i.e., the source spectrum is harder than the diffuse electron spectrum; $C_{e+}/C_{e-} = 0.091 \pm 0.001$, i.e., the weight of the diffuse positron flux amounts to ∼10% of that of the diffuse electron flux; $C_s/C_{e-} = 0.0078 \pm 0.0012$, i.e., the weight of the common source constitutes only ∼1% of that of the diffuse electron flux; $1/E_s = 0.0013 \pm 0.0007$ GeV^{-1}, corresponding to a cutoff energy of 760^{+1000}_{-280} GeV.

The fit is shown in Fig. 5 as a solid curve. The agreement between the data and the model shows that the positron fraction spectrum is consistent with $e^{\pm}$ fluxes each of which is the sum of its diffuse spectrum and a single common power law source. No fine structures are observed in the data. The excellent agreement of this model with the data indicates that the model is insensitive to solar modulation effects [9] during this period. Our study also shows that the slope of the positron fraction as a function of energy decreases by an order of magnitude from 20 to 250 GeV.

2.2. The positron and electron spectrum

The behavior of the positron ratio at energies above 20 GeV observed by AMS-02 can be further studied by analyzing independently the positron and electron spectra [10] as well as the sum of the two spectra [11] in the same energy range.

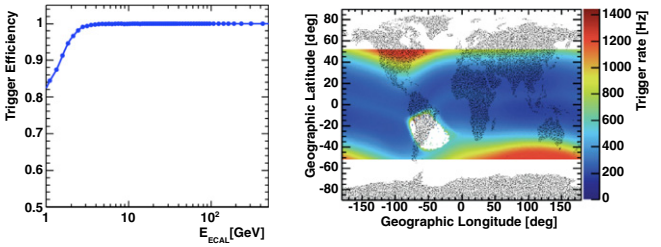

Fig. 6. Left: trigger efficiency for electrons as a function of energy. Right: Trigger rate as a function of orbital position. Variations are correlated with the geomagnetic cutoff rigidity.

The flux of cosmic-ray electrons or positrons $\phi e_{\pm}$ in energy bins ΔE can be determined as

$$\phi_{e\pm} = N_{e\pm}/(A_{eff} \cdot \varepsilon_{\rm trig} \cdot \varepsilon_{\rm sel} \cdot T \cdot \Delta E) \quad (3)$$

with the number of measured electrons or positrons $N_{e\pm}$, the effective acceptance $A_{\rm eff}$, trigger efficiency $\varepsilon_{\rm trig}$, selection efficiency $\varepsilon_{\rm sel}$, and measurement time T. The width ΔE of the energy bins are chosen sufficiently large with respect to the energy resolution of the ECAL. This minimizes necessary corrections to the fluxes by unfolding. At high energies still larger bin sizes ensure sufficient counting statistics in each bin. The event numbers $N_{e\pm}$ in each bin are evaluated a similar procedure as described in the analysis of the positron ratio. A loose preselection is used to define measurement times of stable detector operations for the whole data set. Further quality cuts define a high quality data set with excellent and unambiguous event reconstruction. Events are selected by requiring a track in the TRD and in the tracker, a cluster of hits in the ECAL, and a measured velocity $b > 0$ in the TOF consistent with a downward-going $Z = 1$ particle. 30 million events pass this selection. Above the energy scale of geomagnetic cutoff and solar modulation the raw spectrum is a straight power law, also for the distinct event classes with positive and negative reconstructed charge sign. The ECAL estimator and E/R matching are used to further reject protons. The cuts are chosen to have a high efficiency, but still reduce the proton background significantly. The resulting event samples of electron and positron candidate events are then evaluated by template fits to the distribution of the TRD estimator. By varying the normalizations of signal and background templates, the template fits for positive and negative rigidities determine the total number of positrons and electrons, respectively, in any given energy bin. In this way the analysis utilizes the identification power of the three estimators and determines efficiently the number of electrons and positrons.

The trigger efficiency $\varepsilon_{\rm trig}$ is determined from data. In addition to physics triggered events, AMS records so-called unbiased triggers (with a scaling factor of $f_{\rm PS}$). The trigger efficiency is then given by

$$\varepsilon_{\rm trig} = N_{\rm phys}/(N_{\rm phys} + f_{\rm PS} \cdot N_{\rm unbias}). \quad (4)$$

In Fig. 6 (left) the resulting trigger efficiency is shown as a function of energy. Above an energy of 3 GeV the trigger efficiency is constant and very close to unity.

The AMS trigger rate is shown in Fig. 6 (right). For this analysis we have analyzed data taken from 19 May 2011 to 11 March 2013. For each second, the global status of AMS is defined with several parameters. The exposure time period is selected as follows:

- AMS is in the nominal data taking status.
- AMS vertical axis is within 25_ of the Earth zenith axis, and
- the measured ECAL energy is required to exceed by factor 1.2 the maximal Stoermer cutoff [11].

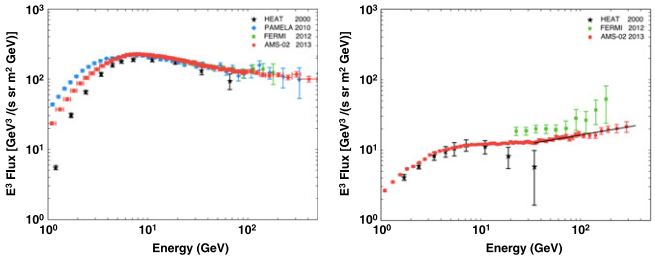

Fig. 7. Electron (left) and positron (right) fluxes as measured by AMS-02. For comparison, data from PAMELA [12], FERMI [8] and HEAT [3] are shown. Data points are positioned within the energy bins according to [13].

The total exposure time depends on the measured ECAL energy and is for energies above 30 GeV constant at $4.38 \cdot 10^7$ s, which corresponds to an overall average live time fraction of 80.2% for this time interval.

The preliminary fluxes multiplied by the third power of the energy are shown in Fig. 7.

The electron flux measurement extends up to 500 GeV. Multiplied by E^3 it is rising up to 10 GeV and appears to be on a smooth, slowly falling curve. The measurement is in good agreement with the previous data reported by the PAMELA experiment [13] and HEAT experiment [14]. The differences at low energies can be attributed to the effect of solar modulation.

The positron flux measurement extends up to 350 GeV. Multiplied by E^3 it is rising up to 10 GeV, from 10 to 30 GeV the spectrum is flat and above 30 GeV again rising as indicated by the black line in the figure. The spectral index and its dependence on energy is clearly different from the electron spectrum. In the low energy range the agreement with results reported by the HEAT experiment [14] is good.

2.3. The all electron spectrum

The measurement of the all-electron spectrum with the AMS-02 detector has been performed at energies between 0.5 and 700 GeV and is shown in Fig. 8 [11]. The assessment of systematic uncertainties is currently being finalized. For this measurement, ∼9 million electrons have been selected from more than 30 billion trigger collected in two years of operation in space. This represents ∼10% of the expected AMS data sample. From this preliminary study, no evidence has been found of structures in the electrons energy spectrum such as those observed by ATIC and PPB-BETS. However, above ∼30 GeV a change in the spectral distribution with increasing electron energies can be seen, which is better appreciated in the separate measurements of the e^- and e^+ components of the flux. In the current understanding of the measurement uncertainties, this change could be compatible with the phenomenological description of the electron and positron components observed in the AMS-02 positron fraction measurement.

3. Conclusions

The accurate measurement of the positron ratio, the electron and positron spectrum and the all electron spectrum, show the physics potential of the AMS-02 experiment in exploiting large statistical samples of CR while keeping the systematic error at the $O(1\%)$ level. Other precision measurements have already been

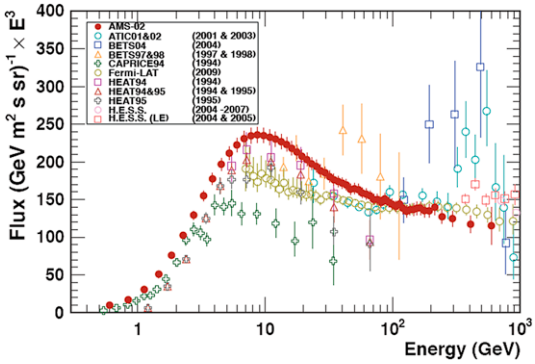

Fig. 8. AMS combined electrons+positron spectrum (full circles) superimposed to existing measurements [15–19].

presented by the AMS Collaboration and more are expected in the future, e.g. proton spectrum [20], helium spectrum [21], B/C ratio spectrum [22] and positron ratio anisotropy [23]. Due to space limitation we refer to the published papers for the details.

After one hundred years from their discovery, thanks to AMS-02 we are finally entering the era of precision Cosmic Ray physics and we can start searching for new phenomena using the kind of cosmic radiation which was discovered first.

Acknowledgments

This work has been supported by acknowledged person and institutions in [1] as well as by the Italian Space Agency (ASI) under contract ASI-INFN I/002/13/0 and ASDC/011/11/1.

References

[1] M. Aguilar, et al., Phys. Rev. Lett. 110 (2013) 141102.
[2] P.D. Serpico, Astropart. Phys. 39 (40) (2012) 2;
T. Delahaye, et al., Astron. Astrophys. 501 (2009) 821;
I. Moskalenko, A. Strong, Astrophys. J. 493 (1998) 693.
[3] R. Golden, et al., Astrophys. J. 457 (1996) L103.
[4] M. Boezio, et al., Adv. Space. Res. 27 (4) (2001) 669.
[5] J.J. Beatty, et al., Phys. Rev. Lett. 93 (2004) 241102;
M.A. DuVernois, et al., Astrophys. J. 559 (2001) 296.
[6] M. Aguilar, et al., Phys. Lett. B 646 (2007) 145.
[7] O. Adriani, et al., Astropart. Phys. 34 (2010) 1;
O. Adriani, et al., Nature 458 (2009) 607.
[8] M. Ackermann, et al., Phys. Rev. Lett. 108 (2012) 011103.
[9] I. Usoskin, et al., J. Geophys. Res. 116 (2011) A02104;
Y. Asaoka, et al., Phys. Rev. Lett. 88 (5) (2002) 051101-1.
[10] S. Schael, AMS Collaboration, Precision measurements of the electron spectrum and the positron spectrum with AMS, in: Proceedings 33rd ICRC, Rio de Janeiro, 2013.
[11] B. Bertucci, AMS Collaboration, Precision measurement of the $e^+ + e^-$ spectrum with AMS, in: Proceedings 33rd ICRC, Rio de Janeiro, 2013.
[12] C. Stoermer, The Polar Aurora, Oxford University, London, 1950.
[13] O. Adriani, et al., Phys. Rev. Lett. 106 (2011) 201101.
[14] M.A. DuVernois, et al., ApJ 559 (2001) 296.
[15] J. Chang, et al., Nature 456 (2008) 362–365.
[16] S. Torii, et al. arxiv:0809.0760.
[17] M. Ackerman, et al., Phys. Rev. D 82 (2010) 092004.
[18] F. Aharonian, et al., Phys. Rev. Lett. 101 (2008) 261104.
[19] F. Aharonian, et al., A&A 508 (2009) 561–564.
[20] S. Haino, AMS Collaboration, Precision measurement of the proton flux with AMS, in: Proceedings 33rd ICRC, Rio de Janeiro, 2013.
[21] V. Choutko, AMS Collaboration, Precision measurement of the cosmic ray helium flux with AMS experiment, in: Proceedings 33rd ICRC, Rio de Janeiro, 2013.
[22] A. Oliva, AMS Collaboration, Precision measurement of the cosmic ray boron-to-carbon ratio with AMS, in: Proceedings 33rd ICRC, Rio de Janeiro, 2013.
[23] J. Casaus, AMS Collaboration, Precision measurement of the cosmic ray boron-to-carbon ratio with AMS, in: Proceedings 33rd ICRC, Rio de Janeiro, 2013.